buildings

MDPI

Article

Reinforcement of Timber Beams with Steel Bars: Parametric Analysis Using the Finite Element Method

André Luis Christoforo [1], Arthur Filipe Freire Gomes [1], Felipe Nascimento Arroyo [1,*], Fernando Júnior Resende Mascarenhas [1], Herisson Ferreira dos Santos [2], Luciano Topolniak [2] and Jorge Luis Akasaki [3]

[1] Department of Civil Engineering, Federal University of São Carlos, São Carlos 13565-905, SP, Brazil; christoforoal@yahoo.com.br (A.L.C.); arthurfreire2009@gmail.com (A.F.F.G.); fer.jr.resende@hotmail.com (F.J.R.M.)
[2] Federal Institute of Education Science and Technology of Rondônia, Vilhena 76980-000, RO, Brazil; herisson.santos@ifro.edu.br (H.F.d.S.); luciano.topolniak@ifro.edu.br (L.T.)
[3] Department of Civil Engineering, Júlio de Mesquita Filho State University of São Paulo, São Paulo 01049-010, SP, Brazil; jorge.akasaki@unesp.br
* Correspondence: lipe.arroyo@gmail.com; Tel.: +55-(17)-99284-2500

Abstract: Incorporating steel bars as reinforcement in glued laminated timber beams is a technique that aims at better structural performance, allowing the reduction of cross-sections. In the present research, based on experimental results from literature about the reinforcement of timbers beams, a parametric study was carried out with the aid of 164 numerical simulations performed within the scope of linear and nonlinear physical analysis via the finite element method to evaluate, with the aid of analysis of variance (ANOVA), the span, base, height, and the reinforcement ratio influence in the service force, ultimate force, and ultimate displacement. Multiple regression models evaluated by ANOVA were established to estimate the service and ultimate forces and ultimate and service displacements as a function of other variables. The results showed an average increase in the service load of 32% and 49%, and the ultimate load of 42.90% and 66.90%, for reinforcement rates of 2% and 4%, respectively. Regarding the multiple regression models, due to the good values obtained from the adjusted determination coefficients to estimate the values of the forces and the ultimate displacements, these can be used in the pre-design of glued laminated timber beams reinforced with steel bars.

Keywords: structural reinforcement; ABAQUS; Hill's failure criteria; ANOVA

Citation: Christoforo, A.L.; Gomes, A.F.F.; Arroyo, F.N.; Mascarenhas, F.J.R.; Santos, H.F.d.; Topolniak, L.; Akasaki, J.L. Reinforcement of Timber Beams with Steel Bars: Parametric Analysis Using the Finite Element Method. *Buildings* **2022**, *12*, 1036. https://doi.org/10.3390/buildings12071036

Academic Editor: Nerio Tullini

Received: 2 June 2022
Accepted: 5 July 2022
Published: 18 July 2022

1. Introduction

Currently, due to global warming and the growing concern with sustainable development, natural materials have become increasingly attractive [1], as is the case for timber used in civil construction [2]. However, wood beams are generally underutilized due to natural defects and usually present premature fragile rupture in the tensile zone [3].

However, some factors reinforce its feasibility of use, such as the relationship between good mechanical behavior and reduced own weight, and because it is a renewable raw material. Although wood has these advantages, its heterogeneity and low rigidity limit its use in certain structural members, such as beams with large spans. Thus, techniques that aim to standardize its properties are increasingly widespread [4], such as the proposal of glued laminated timber (GLT) and the use of reinforcements.

Technological advances have promoted the development of new equipment and methods for wood processing, increasing its quality and reliability. Among the several advances, it is possible to highlight the improvement of the GLT manufacturing process, which expanded the use of structural timber elements in civil construction. The GLT

manufacturing process produces elements with greater stiffness, less material variability, and natural timber imperfections, like knots [5].

According to Soriano et al. [4], the wood used in the production of GLT is generally from fast-growing trees with low density, which consequently results in pieces with low modules of elasticity. This fact emphasizes the need for the use of reinforcement materials that increase the stiffness of the wood element. Yang et al. [6] pointed out that a timber beam presents greater deflections when compared to steel or reinforced concrete beams with the same dimensions and subjected to the same loads. Therefore, the use of GLT is directly limited by the service limit state of the structure, which implies that the strength of GLT beams is partially updated, especially under compression stress [7]. Because of this, different types of reinforcements have emerged and been applied to promote improvements in GLT beams that aim to increase the stiffness of the elements [4,8].

Among the most commonly used techniques for reinforcement in timber structures, it is possible to mention at least two of the most widely used: polymers reinforced with fiber (PRF) and metallic reinforcement (usually through exposed plates that are fixed on the face with tensile or compression). The fibers present excellent tensile strength, being predominantly applied as reinforcement in the tensile region. In contrast, the characteristics of steel make it quite versatile, mainly because it presents a similar behavior when subjected to compression and tension. Due to the advantages provided for mechanical performance, reinforced timber has been the subject of numerous research studies.

Borri et al. [9] elaborated an experimental program to evaluate timber beams reinforced with a unidirectional carbon fiber fabric. Their responses regarding stiffness, ductility, and strength were analyzed. The authors found that the reinforced timber presented significantly better responses in stiffness and load capacity in bending. Neubauerová [10] also studied the possibility of strengthening wood beams with polymer lamellas and carbon fibers distributed in the matrix.

Ghanbari-Ghazijahani et al. [11] conducted an experimental and numerical investigation to analyze the shear and bending strengths of lightweight composite I-beams built of timber to improve their structural behavior by reinforcing them with composite material. The authors observed that there was an enhancement in the ductility, energy absorption, and load capacity of the reinforced timber beams.

Raftery and Whelan [12] evaluated beams produced with glued laminated timber reinforced with fiberglass bars and observed that the use of a percentage of 1.4% of reinforcement promoted an increase of 11.2% in the overall stiffness of the member and an increase of 68% in the capacity of the final bending moment. Raftery and Kelly [13] evaluated the behavior of glued laminated timber beams reinforced with basaltic fibers as an alternative to reinforcement material. An improvement was also noted in the member's overall stiffness and ultimate force capacity for a low reinforcement percentage, with an increase of 23% at the maximum moment. Hence, this material shows great potential since it is a natural raw material that is more economically viable than carbon fiber and glass.

Even so, the reinforcement of timber structures is generally made with metal, either in the form of leaves, plates (more usual), or bars (with the possibility of protection of the bars against the action of fire). Highlighting the reinforcement with steel bars, where few works are published in the related literature, Luca and Marano [14] analyzed experimentally and numerically GLT beams reinforced with simple and pre-tensile steel bars, with a steel-to-wood ratio of 0.82%. The results obtained by the authors proved that in both cases of reinforcement, there was an increase in stiffness and load capacity, with an increase of 40.2% for the prestressed configuration and 48.1% for beams without prestressing.

Soriano et al. [4] developed a study in which GLT beams reinforced with steel bars in the proportions of 2% and 4% were tested. The results showed that the beam with the lowest reinforcement rate showed an improvement of 52% in terms of stiffness and 53.1% in terms of service load. The benefits of the beam with the highest reinforcement rate were 73% and 79.2%, respectively.

Yang et al. [6] carried out experimental and theoretical programs of GLT beams with different types, arrangements, and reinforcement rates. Reinforced beams were analyzed with glass fiber, steel bars, and laminated composites (plates) in fiberglass and carbon, with reinforcement rates from 0% (control) to 1.787% of the cross-section. The ultimate bending moment showed 56.3% higher values for the reinforcement of the carbon fiber plate located in the tensile zone. Reinforcements with fiberglass bars located in the tensile and compression regions showed an increase of 34.1% (rate of 1.787%). Similar results were found by Mcconnell et al. [15] with an increase of 30% in the last load, using bars in the tensile region with a rate of 1.67%.

Concerning the methodology for calculating GLT beams reinforced with steel bars, reduced information is found in the literature, with a lack of studies that make it possible to estimate the load that a reinforced beam resists or show how to determine which parameters mainly influence the improvement of the mechanical characteristics of the reinforced structure. In this sense, the biggest obstacle that makes designers hesitate to use certain materials is the lack of knowledge of their mechanical behavior [16].

The lack of experimental data on the mechanical behavior of GLT elements reinforced with steel bars can be overcome using numerical tools such as the finite element method (FEM). For that, it is important to adopt adequate constitutive relationships, failure criteria, and intrinsic relationships between mechanical strength properties [17]. Thus, it is possible to evaluate the reinforced structures mainly in the ultimate limit state condition, allowing designers greater sensitivity about the security level of the structures to be designed.

Therefore, given the benefits that reinforcement with steel bars has for GLT elements, and the absence of extensive information in the literature concerning the influence of each variable in the mechanical behavior of these materials together, and the orthotropy of wood, parametric studies present important fields of research, either in offering insights into the most influential parameters or in the definition of mathematical models for the estimation of variables involved in the design of GLT elements reinforced with steel bars.

Based on experimentally validated modeling (results published in the related literature), this research aimed, through a parametric study (164 simulations in total) that is essentially numeric via the finite element method, which was performed through linear and nonlinear physical and geometric analysis, analysis of variance (ANOVA), and multiple regression models also evaluated by ANOVA, to investigate the influence of the dimensions of the timber beams (base—b; height—h; length—L) and the reinforcement rate (%s) on the values of the ultimate (Fu) and service (Fs) forces (loads) and ultimate displacement (δu). Models were established to estimate the forces (Fu and Fs) and the ultimate displacement as a function of other variables, allowing the design engineer to estimate the loads and displacements for values of the independent variables not included in the parametric study.

2. Materials and Methods

In order to analyze the behavior of beams reinforced with steel bars, numerical models were developed in the SIMULIA Abaqus [18] software. Such models were validated based on the experiments carried out by Luca and Marano [14], which consisted of a series of four-point bending tests of reinforced timber beams with steel bars in the tensile and compression zone and timber beams with no reinforcement (unreinforced) (Figure 1).

After validating the model, a parametric study was carried out to evaluate the influence of the dimensions of the reinforced timber beams (L, b, h), reinforcement rate (%s), and limit displacement in the service condition (δs) under the values of the ultimate (Fu) and service (Fs) loads and ultimate displacement (δu). In addition, models were established to estimate loads (Fu and Fs) and displacements (δs and δu) as a function of other variables. As mentioned, the methodology of this work consisted of numerical simulations carried out within the scope of linear and nonlinear physical and geometric analysis via FEM, analysis of variance (ANOVA), and multiple regression models also evaluated by ANOVA.

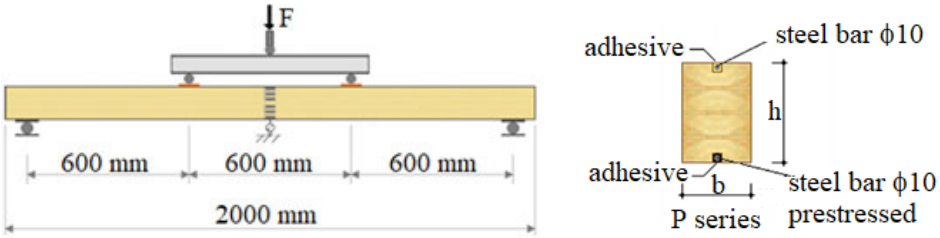

(**a**) (**b**)

Figure 1. Considered dimensions in the: (**a**) four-point bending test; and (**b**) details of the cross-section with the inclusion of steel bars. Source: Adapted from Luca and Marano [14]. Reprinted/adapted with permission from Ref. 5344251152086.

2.1. Parametric Study

In order to generate high-quality equations (R^2 close to 1–100%), a comprehensive parametric study was developed. The independent variables adopted were the beam length (L), base (b), height (h), reinforcement rate (%s), bar diameter (d), and the limit displacement considered for the condition of service limit state (δs). The variations followed the underlying assumptions:

i. Length (L): 2000 mm; 5000 mm; and 10,000 mm
ii. Base (b): 20 different values were adopted, ranging from 33.33 mm to 233.33 mm. For better results representation, the values were grouped into 5 classes: between 0 mm and 50 mm; between 50 mm and 100 mm; and so on, until the range between 200 mm and 250 mm. The 20 values adopted were equally distributed among the 5 classes adopted;
iii. Height (h): 100 mm, 150 mm, 200 mm, 250 mm, 300 mm, and 350 mm;
iv. Reinforcement rate (%s): 0; 2; and 4%, being the limit indicated by Soriano, Pellis, and Mascia [4];
v. Steel bars diameter (d): following the same assumptions as for the basis (b), 40 different diameter values were adopted, ranging from 0 mm to 45.60 mm. For better results representation, the values were grouped into 5 classes: between 0 mm and 10 mm; between 10 mm and 20 mm; and so on, until the range between 40 mm and 50 mm. The 40 values adopted were equally distributed among the 5 classes adopted. It is worth pointing out that the reinforcement rate was respected in all cases;
vi. Displacement (δs): the displacement limits were 10 mm, 25 mm, and 50 mm for the lengths (L) of 2000 mm, 5000 mm, and 10,000 mm, respectively. It should be noted that the limit stipulated by the Brazilian standard ABNT NBR 7190 [19] "Design of Timber Structures" of $L/200$ was respected.

The combination of the levels of the factors considered generated 164 different treatments, and 164 numerical simulations were carried out. The response variables obtained consisted of the forces determined in the service (Fs) and ultimate (Fu) conditions as well as the ultimate (δu) and service (δs) displacements.

The Tukey test, at the 5% level of significance, was used to verify the influence of each factor (L, $\%s$, h, b, d, δs) on the values of the selected response variables (Fs, Fu, δu). Subsequently, regression models (Equation (1)) were used in order to relate the response variables to the considered factors (L, $\%s$, h, b, d) in the parametric study. These models were evaluated by analysis of variance (ANOVA), also at the 5% level of significance, which allows the determination of the models' significance and the component terms of those models (sensitivity analysis).

$$Y = \beta 0 + \beta 1 \times s + \beta 2 \times h + \beta 3 \times b + \beta 4 \times d + \beta 5 \times \%s2 + \beta 6 \times h2 + \beta 7 \times b2 + \beta 8 \times d2 + \beta 9 \times \%s \times h + \beta 10 \times \%s \times b + \beta 11 \times \%s \times d + \beta 12 \times h \times b + \beta 13 \times h \times d + \beta 14 \times b \times d + \varepsilon \quad (1)$$

From Equation (1), Y consists of the response variables (Fs, Fu, δu, δs), βi are the coefficients adjusted by the method of least squares, and ε is the random error. It is worth noting that the accuracy of the models was assessed using the adjusted determination coefficient (R^2 adj).

2.2. Numerical Model Validation

Three-dimensional numerical models were developed using the SIMULIA Abaqus [18] software (based on the finite element method—FEM) to simulate the flexural behavior of reinforced beams with the insertion of steel bars in the tension and compression regions.

The proposed numerical methodology was validated based on the experimental work developed by Luca and Marano [14]. The behavior of glued laminated timber beams of dimensions 80 mm × 117 mm in the cross-section and 2000 mm in length were evaluated (Figure 1).

As the main objective was to analyze the difference in the behavior of reinforced beams in relation to unreinforced beams (influence of the insertion of steel bars), the models were calibrated based on the results of six tested beams, three with no reinforcement and another three with reinforcement (bars positioned at the midpoint of the width of the cross-section and approximately 5 mm of coverage of the lower and upper faces of the beams). The properties related to the wood *Picea glauca* (Canadian pine) and steel bars are shown in Tables 1 and 2, respectively. The loading was applied slowly (4 mm/min) and progressively surpassed the peak load after failure, and the tests were carried out with the displacement control. More details about the characterization of the materials and the conditions of the tests can be found in the research of Luca and Marano [14].

Table 1. Manufacturer specifications regarding the strength and rigidity properties of laminated timber. Adapted from Luca and Marano [14].

Properties	Values (MPa)
Bending strength, the characteristic value	28.00
Tensile strength parallel to the fiber, characteristic value	19.50
Tensile strength perpendicular to the fiber, characteristic value	0.45
Compression parallel to the fiber, characteristic value	26.50
Compression perpendicular to the fiber, characteristic value	3.00
Shear strength, the characteristic value	3.20
Modulus of elasticity parallel to the fiber, average value	12,600
Modulus of elasticity parallel to the fiber, 5% fractile value	10,200
Modulus of elasticity perpendicular to the fiber, average value	420
Tangential modulus of elasticity, average value	780

Table 2. Steel bars' mechanical properties. Source: Luca and Marano [14].

Properties	Mean Value	Characteristic Value (5%)
Ultimate tensile stress (MPa)	675.80	425.20
Ultimate compressive stress (MPa)	1510	1091.20
Ultimate tensile strain (dimensionless)	0.2256	0.1970
Ultimate compressive strain (dimensionless)	0.4944	0.4100
Modulus of elasticity in tension (MPa)	342,375	213.19
Modulus of elasticity in compression (MPa)	342,588	205,238

2.3. Numeric Model Settings

Due to the geometry of the experimental test, symmetry in the longitudinal direction was used in the numerical simulation, allowing the modeling of half of the beam, thus reducing the computational effort and consequently the processing time. Luca and Marano [12] considered that in the region of load application (Figure 1), a steel plate was adopted for stress distribution, with 15 mm in height, 50 mm in length, and 80 mm in width. The model configuration is shown in Figure 2.

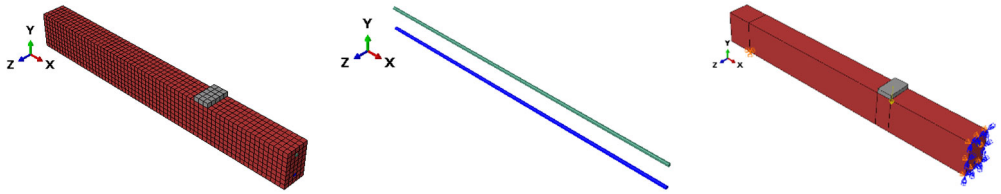

(**a**) (**b**) (**c**)

Figure 2. Representation of the: (**a**) model configuration; (**b**) control (prescribed displacements); and (**c**) loading conditions.

In the finite element mesh of the plate to the load application and the timber beam, solid elements of the C3D8 type were used, with full integration, composed of 8 nodes and linear interpolation, available from the SIMULIA Abaqus [18] internal library.

After a mesh sensitivity analysis (progressive mesh refinement test), the maximum global size of 15 mm was adopted for the two parts (plate and half of the beam), totaling 15 elements for the plate and 2640 elements for the timber beam.

To simulate the bar elements, T3D2 elements were used, also available in the SIMULIA Abaqus [18] internal library, which is a linear geometry element consisting of 2 nodes and 3 degrees of freedom per node. According to the consulted bibliography, with similar studies and materials to those carried out in this work, these elements are the most suitable for discretizing timber and steel bars [3,20–22]. The discretized model is shown in Figure 2. For spans of 5000 mm and 10,000 mm, the maximum total mesh size of 30 mm was adopted to optimize the processing time.

In all numerical simulations involving reinforcement, the steel bars had their geometric centers positioned at half the width and 25 mm from the upper and lower faces of the cross-section.

The punctual loading was applied to the plate incrementally, distributed in the timber beam's contact area. Control conditions were applied to the central support axis, with restricted displacements in the Y and Z directions (Figure 2a,b). As half of the beam was modeled, conditions related to symmetry were applied, with the displacement of the cross-sectional displacements located at the midpoint of the beam length in the X direction (Figure 2c).

The adhesion of the plate to the timber beam was considered a complete iteration, i.e., the contact surfaces of the two materials did not present relative displacement, as occurred in the experiments developed by Luca and Marano [14]. Such behavior was obtained using the "Tie" constraint, available in the SIMULIA Abaqus [18] library. Furthermore, in the experiments of Lucas and Marano [14], there were no failures due to the sliding of the steel bars (surrounded by epoxy resin) in relation to timber for any loading stage, demonstrating the efficiency of the adhesive. As a result, the "Embedded" constraint was used to insert the bars inside the timber beam, which guarantees total adhesion between both elements.

The loading was applied incrementally (Newton–Raphson method) due to the consideration of physical and geometric nonlinearity. The load increments were automatically controlled by the SIMULIA Abaqus [18] software based on the definition of the initial increment of 0.001, a maximum number of 1000 increments, and a tolerance of 10^{-5} for model convergence.

2.4. Constitutive Models

Four material models were adopted in the numerical simulations to represent the following elements: the plate for transferring the load to the beam, the lower steel bar, the upper bar, and the timber.

For the loading transfer plate, it was considered a model of a linear isotropic elastic material with a modulus of elasticity and Poisson's coefficient of 210,000 MPa and 0.3, respectively [23].

The constitutive relationship used for the two steel bars followed the von Mises criterion, commonly used to verify failure in ductile materials. The constitutive model for the steel bars was the elastic–perfectly plastic model (Figure 3a); however, to avoid problems resulting from possible numerical instabilities, a small slope of the curve (modulus of elasticity to 0.053% and 0.020% of the initial value in the compression and tensile bars, respectively) was considered after plasticization stress (f_y), as considered in other works [24,25]. The properties of the upper (compression) and lower (tensile) bars are shown in Table 3.

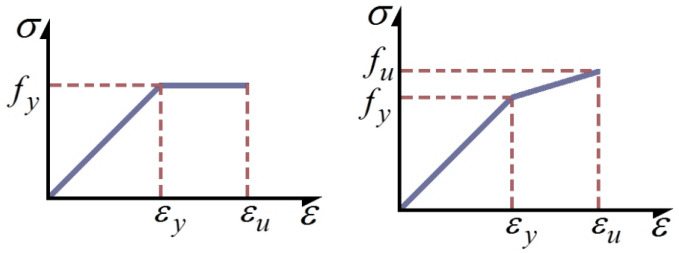

Figure 3. The representation of the: (**a**) adopted constitutive model for reinforcement steel; and (**b**) and timber.

Table 3. Steel bar elastic and plastic properties. Source: Luca and Marano [14].

Elastic Properties			
Property	**Value**	**Property**	**Value**
Ultimate compressive stress (MPa)	1091.2	Ultimate tensile stress (N/mm^2)	425.20
Poisson's ratio	0.30	Poisson's ratio	0.30
Modulus of elasticity in compression (N/mm^2)	205,238	Modulus of elasticity in tension (N/mm^2)	213,190
Plastic properties			
Property	**Value**	**Property**	**Value**
Stress (N/mm^2)	Poisson's ratio	Stress (N/mm^2)	Poisson's ratio
1091.20	0	425.20	0
1102.10	0.10	429.50	0.10

Wood is an orthotropic material and requires knowledge of several properties for its characterization in both elastic and plastic behavior. Without the proper definition of the constitutive model for wood, mechanical behavior and failure modes cannot be accurately predicted by finite element models [26].

For wood, similar behaviors were adopted for the radial and transverse direction; this same condition has been used by several authors as reported in [27,28]. An orthotropic elastoplastic constitutive model with a bilinear curve was used, which was associated with Hill's [29] resistance criterion and isotropic hardening to consider the timber hardening behavior.

The representation of wood by means of elastoplastic behavior associated with hardening has been adopted by several authors, providing satisfactory numerical results [30–32]. A reduction in the modulus of elasticity to 7% of the initial value (10,200 MPa—Table 1) was assumed from stress values greater than 25% of the resistance (26.50 MPa—Table 1) of the timber in the compression parallel to the fibers [24,25].

Hill's [29] criterion is an extension of von Mises's criterion and seeks to consider the anisotropy of materials expressed in terms of cartesian rectangular stress components (Equation (2)). In the case of Hill's [29] criterion, in which the longitudinal, radial, and tangential directions corresponded, respectively, to the X, Y, and Z axes, it is not possible to take into account different values of tensile and compression strength of the wood. As a result, the criterion does not consider fragile failures caused by tensile or shear [33]. However, Hill's anisotropic plasticity criterion has been used for wood simulation, in which good results have been obtained [34–36].

$$f = \sqrt{F \times \sigma_{22} - \sigma_{33})^2 + G \times (\sigma_{33} - \sigma_{11})^2 + H \times (\sigma_{11} - \sigma_{22})^2 + 2 \times L \times +2 \times M \times {\sigma_{31}}^2 + 2 \times N \times {\sigma_{12}}^2} \quad (2)$$

$$F = \frac{1}{2} \times \left(\frac{1}{{R_{22}}^2} + \frac{1}{{R_{33}}^2} - \frac{1}{{R_{11}}^2} \right) \quad (3)$$

$$G = \frac{1}{2} \times \left(\frac{1}{{R_{33}}^2} + \frac{1}{{R_{11}}^2} - \frac{1}{{R_{22}}^2} \right) \quad (4)$$

$$H = \frac{1}{2} \times \left(\frac{1}{{R_{11}}^2} + \frac{1}{{R_{22}}^2} - \frac{1}{{R_{33}}^2} \right) \quad (5)$$

$$L = \frac{3}{2 \times {R_{23}}^2} \tag{6}$$

$$M = \frac{3}{2 \times {R_{13}}^2} \tag{7}$$

$$N = \frac{3}{2 \times {R_{12}}^2} \tag{8}$$

From Equation (2), *F*, *G*, *H*, *L*, *M*, and *N* are constants defined according to Equations (3)–(8), respectively, where σ_0 is reference stress, adopted as the compressive strength parallel to the fibers (σ_{11}), σ_{22} and σ_{33} are the compressive strengths perpendicular to the wood fibers, and σ_{12}, σ_{13}, and σ_{23} are the shear strengths of the wood in planes 1-2, 1-3 and 2-3, respectively.

The ratio between the compressive strength perpendicular to the wood fiber ($\sigma_{90} = \sigma_{22} = \sigma_{33}$) and the compressive strength parallel to the fibers ($\sigma_0 = \sigma_{11}$) is defined as 0.12, according to the premises of EN 338 [37]. The ratio between the shear strength of wood ($\sigma_v = \sigma_{12} = \sigma_{13} = \sigma_{23}$) and the compressive strength parallel to the fibers ($\sigma_0 = \sigma_{11}$) is set to 0.25, according to the premises of NBR 7190 [19].

To characterize the wood behavior, it is necessary to define the modulus of elasticity, transverse modulus of elasticity, and Poisson's coefficients in the longitudinal, radial, and transverse directions. The relationships between these parameters were obtained from EN 338 (CEN, 2009) and Molina and Calil Junior [38] and are presented in the following Equations (9)–(12):

$$E_2 = E_3 = \frac{E_1}{30} \tag{9}$$

$$G_{12} = G_{13} = G_{23} = \frac{E_1}{16} \tag{10}$$

$$\nu_{12} = \nu_{13} = 0.013 \tag{11}$$

$$\nu_{23} = 0.23 \tag{12}$$

Of these equations, E_1, E_2, and E_3 represent the modulus of elasticity in the longitudinal, radial, and tangential directions, G_{12}, G_{13}, and G_{23} represent the transverse modulus of elasticity in planes 1-2, 1-3, and 2-3, respectively, and ν_{12}, ν_{13}, and ν_{23} represent the Poisson coefficients in planes 1-2, 1-3, and 2-3, respectively.

Finally, the relations between the normal stresses of plasticization in the different directions were taken based on the Brazilian code NBR 7190 [19] as being 25%, while the shear stresses (τ) were stipulated as 25% in the XY (longitudinal-radial) and XZ (longitudinal–tangential) planes and 2.50% in the YZ (radial–tangential) plane, as shown in Table 4. The bilinear model of the stress–strain curve in the parallel direction of the fibers was defined by the ultimate stress, or compressive strength tension obtained based on the research by Luca and Marano [14].

Table 4. Plasticity coefficients.

Coefficients	Values
R_{11}	1
R_{22}	0.25
R_{33}	0.25
R_{12}	0.25
R_{13}	0.25
R_{23}	0.025

Poisson's coefficients and elasticity modules are required when using the elastic-orthotropic model. The relationships between elastic properties were admitted based on the work of [24,38,39] and the NBR 7190 [19] timber standard, as already mentioned. The modulus of elasticity to compression in the longitudinal direction (Table 1) was adopted from the work of Luca and Marano [14]. A summary of the elastic properties is shown in Table 5.

Table 5. Elastic properties and relations between admitted properties.

Properties	Values
$\nu_{xy} = \nu_{xz}$	0.013
ν_{yz}	0.23
E_x	9612 MPa
$E_y = E_z$	$E_x/30$ = 320.4 MPa
$G_{xy} = G_{yz} = G_{yz}$	$E_x/16$ = 600.75 MPa

3. Results and Discussion

3.1. Validation of Models

Figure 4 shows the load vs. vertical displacement of the reinforced beam span obtained through numerical simulation and the values obtained experimentally (3 reinforced beams, entitled R1, R2, and R3) by Luca and Marano [14]. The curve obtained via numerical simulation was plotted to the maximum point where the convergence of the model occurred with a tolerance of 10^{-5}. The values of the applied force for displacement in the service limit state condition (L/200—L is the useful distance between the end of the static bending test, 1800 mm—Figure 1) established by the Brazilian standard NBR 7190 [19] and for the rupture values of the reinforced beams are shown in Table 6, and it should be noted that T1, T2, and T3 are the beams with no reinforcement (reference), also tested by Luca and Marano [14]. The ductility, which is the mechanical behavior expected of timber beams by incorporating steel bars, was more noticeable in beam R3. Thus, the results of the load vs. displacement curve of beam R3 were used for comparison with the results obtained from the simulation (Table 6).

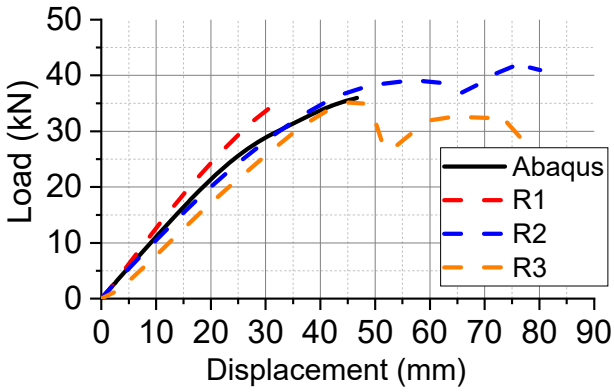

Figure 4. Load curve × displacement for reinforced beam.

Table 6. Comparison between experimental and numerical values for the force at the service and ultimate limit.

Condition		L/200 Load	For the Ultimate Displacement Load
With no reinforcement	T1	10	27.20
	T2	5.40	22.60
	T3	7.10	26.90
	Average	7.50	25.60
	Numeric	10.30	21.70
	Difference	2.90%	−4%
With reinforcement	R1	12.10	36.10
	R2	9.70	39
	R3	7.40	38.60
	Average	9.70	37.90
	Numeric	15.20	36
	Difference	20.60%	−0.30%

Considerable agreement can be seen in Figure 4 and Table 6 between the numerical and experimental results, not only in the linear phase but also in the nonlinear phase when the plasticization mechanism of the materials starts. The maximum experimental and numerical load difference was not more than 8.28%. The behavior of the load vs. displacement curve obtained by the numerical model presented a behavior similar to the curves of the experimental values. In addition, the post-rupture ductile behavior was similar to the one Luca and Marano [12] observed, as the cross-section of the GLT beam showed residual resistance to the loads. The differences observed between the numerical and experimental curves may be due to the non-consideration of imperfections, such as knots and distortions in the fibers. In addition, the timber properties were defined from empirical relationships due to the lack of experimental values.

In the experimental models, the non-reinforced beams failed at the end of the tensile region, causing a sudden loss of resistant section, and the reinforced beams presented a mixed failure of tensile and compression, with cracks in the tensile area and crushing in the compressed one.

Figure 5a,b show the stresses obtained by numerical analysis of the models with no reinforcement and reinforcement, respectively. Considerable plastification of the beam is observed, in which the central region of the span presented stresses equal to or greater than the compressive strength parallel to the fibers (Table 1).

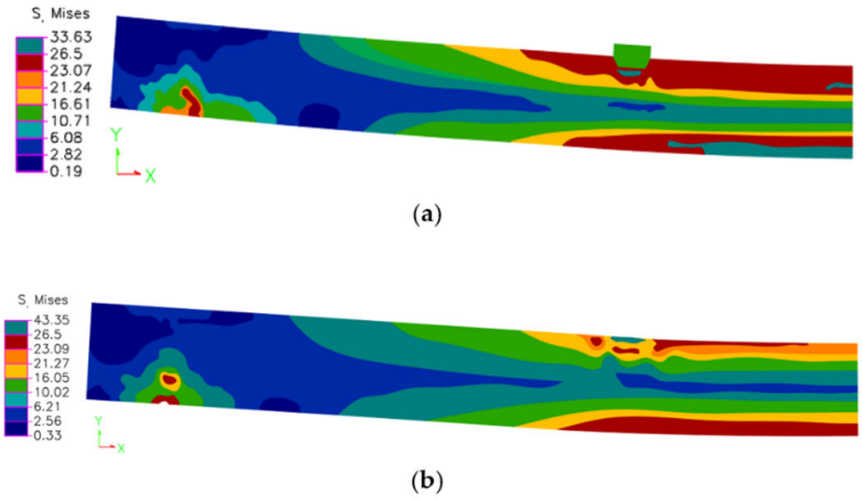

Figure 5. Mises stresses in MPa: (**a**) beam with no reinforcement; (**b**) reinforced beam.

Reinforced beams initially fail in the tensile zone and then crush in the compression zone [14]. Several authors observed such behaviors [2,4,6,13,16,39–42]. Thus, the stresses presented by the numerical model are consistent with the stresses obtained from the experimental model. Figure 6a,b show the stresses in the reinforcement and the maximum vertical displacements of the reinforced beam for the maximum load.

The results show that the proposed numerical models were able to simulate the mechanical behavior of reinforced and unreinforced beams with steel bars in the linear and nonlinear phases. The maximum numerical displacements in the service phase (L (span)/200) and the maximum displacements presented values close to the experimental ones and the respective loads. In addition, the models showed stress concentrations in the experimental rupture regions, demonstrating the model's agreement.

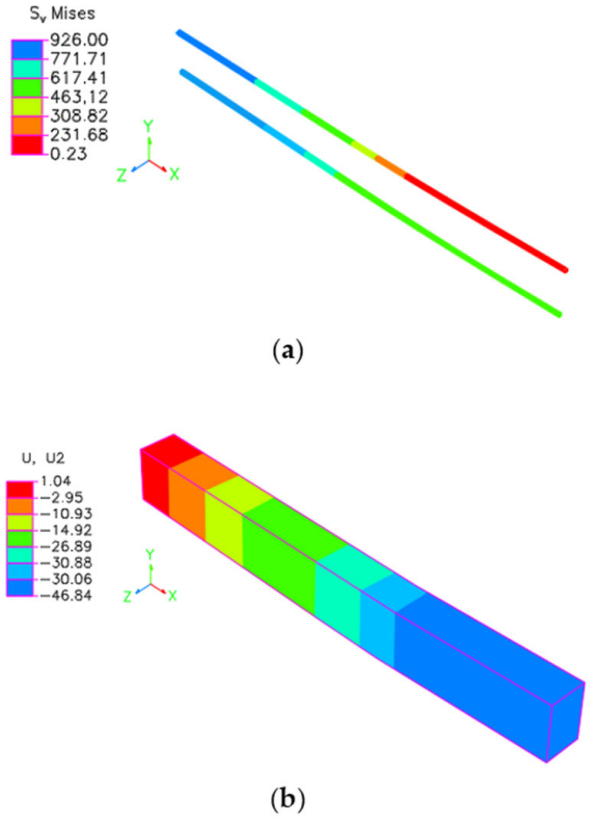

Figure 6. Stresses (MPa) in: (**a**) reinforced wooden beam reinforcement; and (**b**) vertical displacements (mm) of the reinforced wooden beam.

3.2. Parametric Study Results

Figure 7 shows the Tukey test results of the factors (variables considered independent) L, $\%s$, h, b, d, and δs over the response variables (considered dependent) Fs, Fu, and δu, respectively. It must be noted that the variables b (base of the beam cross-section) and d (diameter of the bars) were properly categorized into 5 different classes with an amplitude of 50 mm for variable b and 10 mm for variable d.

$$\begin{cases} 0 \leq b < 50\text{mm} \rightarrow 1 \\ 50 \leq b < 100\text{mm} \rightarrow 2 \\ 100 \leq b < 150\text{mm} \rightarrow 3 \\ 150 \leq b < 200\text{mm} \rightarrow 4 \\ 200 \leq b < 250\text{mm} \rightarrow 5 \end{cases} \text{and} \begin{cases} 0 \leq d < 10\text{mm} \rightarrow 1 \\ 10 \leq d < 20\text{mm} \rightarrow 2 \\ 20 \leq d < 30\text{mm} \rightarrow 3 \\ 30 \leq d < 40\text{mm} \rightarrow 4 \\ 40 \leq d < 50\text{mm} \rightarrow 5 \end{cases}$$

The reinforcement showed an increase of approximately 32% and 49% in the service force values for reinforcement rates of 2% and 4%, respectively, which are lower than the values obtained by Soriano et al. [4], with an increase in the load service of 53.1% and 79% for reinforcement rates of 2% and 4%, respectively. The values of the modulus of elasticity of the wood and the steel reinforcement used by Soriano et al. [4] were different from those defined in this work; however, both studies showed significant increases in the load capacity of the beam. It can be observed that the different reinforcement rates showed statistically equivalent mean service load values, both values being higher than those with no reinforcement, indicating the efficiency of the use of steel bars. Thus, reinforced elements allow the solution of certain load and height limits of the cross-section related to design restrictions. In addition, it was noted that the beam height had a significant influence on the service load, with the heights of 300 and 350 mm showing statistically equivalent mean values. However, the average supported by the 350 mm high beams was substantially higher than the 300 mm beams, resulting in a value of approximately 44%.

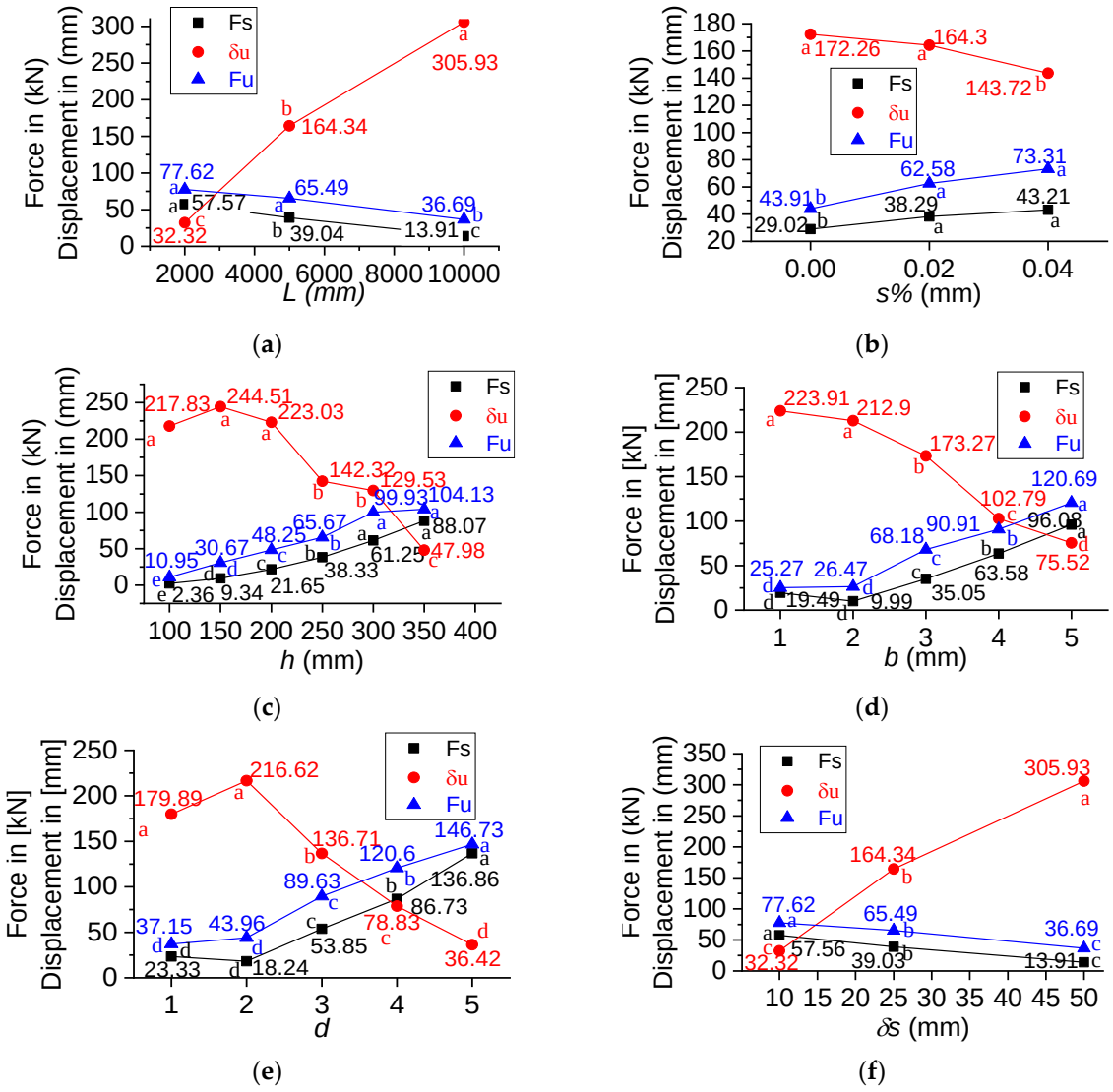

Figure 7. Tukey test results of the variables: (**a**) *L*; (**b**) %*s*; (**c**) *h*; (**d**) *b*; (**e**) *d*; and (**f**) *δs* in relation to the force determined at the limit of the service condition (*Fs*), ultimate force (*Fu*), and last displacement (*δs*). From the Tukey test, at the 5% significance level, "a" denotes the highest mean value of the property, "b" is the second-highest mean value, and so on, and the same letters imply different treatments with statistically equivalent means.

The reinforcement values of 2% and 4% presented average ultimate load values of 42.9% and 66.9%, respectively, when compared with beams with no reinforcement. The values found in this research were higher than those observed by Luca and Marano [14], in which the increase in the ultimate load was 48.1% for a reinforcement rate of 0.82%. The results were also higher than the values obtained by Yang et al. [6] and Chaudhari and Chakrabarti [20], in which the application of fiberglass bars in the stretched and compressed regions increased the final load by approximately 30%.

The increase observed in the present study was also greater than that observed by Raftery and Kelly [13] in beams reinforced with basaltic fibers (an increase of 23% in maximum capacity). In addition, the increase in the ultimate load obtained in this research was similar to that presented by Yang et al. [6], in which the reinforcement with a carbon fiber plate located in the tensile zone showed an increase of approximately 56% in the ultimate load (reinforcement rate of 1.85). Finally, the reinforcement with fiberglass bars showed better performance, increasing the final capacity of the beam by 68% with 1.4% of reinforcement [16]. The fact that the different reinforcement rates have statistically equivalent averages and service loads shows the efficiency of the use of reinforcement, even with a reinforcement rate of 2%.

The results illustrated indicate that the heights of 300 and 350 mm did not show statistical differences from the ultimate load, and did not significantly increase the value of the ultimate load of the structure. Thus, for the models proposed in this research, the height of 300 mm was the most efficient because it presented a load approximately 4% lower than the 350 mm beam. Base (*b*) and diameter (*d*) parameters showed similar behaviors, with categories 1 and 2 showing equivalent average values. As a result, category 1 has more efficient values because it requires less material.

The results obtained show the efficiency of reinforcement with steel bars in the tensile and compression areas, with a significant increase in the ultimate load. In addition, steel bars are easily found, unlike other reinforcements such as synthetic and natural fibers, and they have similar behavior in compression and tensile. All these factors make steel bar reinforcements an efficient alternative to increase the load capacity of GLT timber elements.

Analyzing the last displacements as a function of height, the consideration of 100 mm, 150 mm, or 200 mm in the height value did not promote significant changes in the mean values of δu because they were statistically equivalent to each other. The 250 mm and 300 mm measurements were statistically equivalent to each other but less than 100 mm, 150 mm, and 200 mm. Finally, the height of 350 mm showed the lowest average value.

As expected, beams with a lower height and, consequently, a lower moment of inertia, had the highest values of ultimate displacements. It was also noted that the use of a reinforcement rate of 2% did not significantly modify the average values of δu, being statistically equivalent to each other. In contrast, beams with a reinforcement rate of 4% showed lower mean values of δu. The beams with reinforcement rates showed average displacements lower than 4.5% and 16.6% for reinforcement rates of 2% and 4% when compared to beams with no reinforcement. In addition, reinforcements of categories 4 and 5 in diameter were used in beams with higher heights (300 mm and 350 mm), which justifies the considerably lower mean values of δu.

For a better understanding of the values considered in this research for the measures of the base (*b*) and the diameters (*d*) of the steel bars, which are of fundamental importance for the generation of the regression models, in Figure 8, the respective frequency histograms are presented, with M being the mean, SD the standard deviation and N the number of observations. Figure 8a,b show the frequency of distribution of variables *b* and *h* considered in the simulations (synthesis of the results generated from the simulations), showing that the two variables (*b* and *d*) showed normality in their respective distributions.

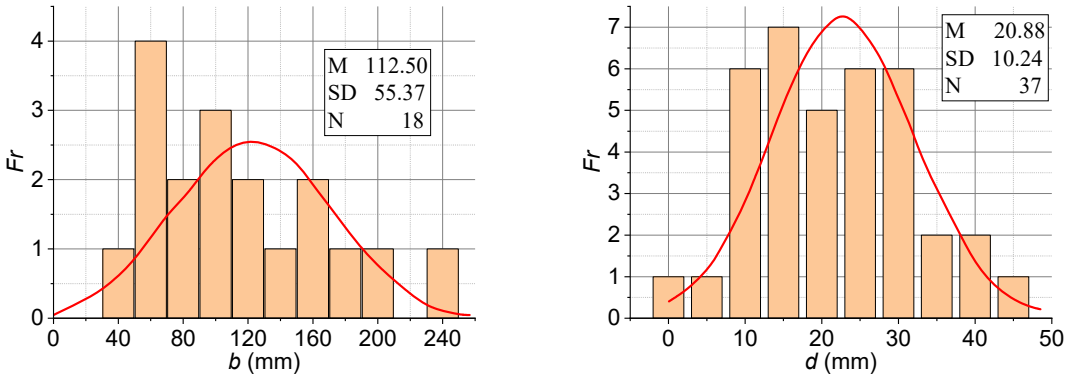

(**a**) (**b**)

Figure 8. Frequency: (**a**) histograms regarding the values of the measurements *b*; (**b**) *d* stipulated for the numerical simulations of the beams.

For the use of the regression models presented below as a way of estimating *Fs*, *Fu*, and δu, the limits of the variables considered dependent must be respected, being these: 2000 mm $\leq$ mm $L \leq$ 10000 mm, 33.33 mm $\leq$ mm $b \leq$ 233.33 mm; 100 mm $\leq$ mm $h \leq$ 350 mm, 0% $\leq$ %$s \leq$ 4%, and 0 mm $\leq$ mm $d \leq$ 45.60 mm. Equations (13)–(16) express the models for estimating δs, *Fs*, *Fu*, and δu, respectively, together with the adjusted determination coefficients (R^2 adj), and in Table 7 are presented, for each of the four adjustments, the significance (*p*-value < 0.05) or not (*p*-value $\geq$ 0.05) of the models and their component terms, and it should be noted that the closer to 0, the more significant the terms and the model are.

$$\begin{gathered}\delta s = 34.6 - 79 \times \%s + 0.007 \times h - 1.9 \times b - 3.69 \times d - 947 \times \%s^2 - \\ 0.000040 \times h^2 - 0.73 \times b^2 + 0.05 \times d^2 - 0.13 \times \%s \times h + 59 \times \%s \times b + \\ 33 \times \%s \times d - 0.0007 \times h \times b + 0.0070 \times h \times d + 0.87 \times b \times d \\ \left[R^2 adj = 3.48\%\right]\end{gathered} \quad (13)$$

$$\begin{gathered}Fs = 1.5 + 117 \times \%s - 0.003 \times h - 0.142 \times b + 2.4 \times d - 570 \times \%s^2 + \\ 0.000154 \times h^2 + 0.00085 \times b^2 + 0.006 \times d^2 - 10.1 \times \%s \cdot h - 19.2 \times \%s \times b + \\ 101 \times \%s \times d + 0.00077 \times h \times b + 0.0033 \times h \times d - 0.0002 \times b \times d \\ \left[R^2\ adj = 68.84\%\right]\end{gathered} \quad (14)$$

$$\begin{gathered}Fu = -21.5 - 630 \times \%s + 0.218 \times h + 0.151 \times b + 8.5 \times d + 2703 \times \%s^2 - \\ 0.000016 \times h^2 + 0.00098 \times b^2 - 0.023 \times d2^2 - 23.5 \times \%s \times h - 49.3 \times \%s \times b + \\ 277 \times \%s \times d - 0.00052 \times h \times b + 0.0014 \times h \times d - 0.0001 \times b \times d \\ \left[R^2\ adj = 74.26\%\right]\end{gathered} \quad (15)$$

$$\begin{gathered}\delta u = 176 + 119 \times \%s + 1.27h - 0.78 \times b + 13.9 \times d - 5893 \times \%s^2 - \\ 0.00454 \times h2^2 - 0.0018 \times b^2 - 0.02 \times d^2 - 45 \times \%s \cdot h - 102 \times \%s \cdot b + \\ 521 \times \%s \times d + 0.0029 \times h \times b - 0.0024 \times h \times d + 0.007 \times b \times d \\ \left[R^2\ adj = 19.51\%\right]\end{gathered} \quad (16)$$

From Table 7, none of the evaluated models were considered significant by ANOVA. The low value associated with R^2 *adj* (3.48%) of the regression model in Equation (13) is because the limit displacements (δs), regardless of other factors, are always equal to 10 mm, 25 mm, or 50 mm ($L/200$). Estimates of better precision were achieved with the models in Equations (6) and (7), and of lower precision in estimating the ultimate displacement (Equation (11)). Even though R^2 *adj* is close to 70% in the models in Equations (14) and (15), these were still considered insignificant by ANOVA, which implies that variations in the independent variables cannot significantly explain the variations suffered by the dependent variables.

Table 7. ANOVA results (p-value) of the regression models expressed by Equations (8)–(11).

Statistics	Equation (5)	Equation (6)	Equation (7)	Equation (8)
Model	0.985	0.476	0.388	0.922
Constant	0.000	0.799	0.526	0.844
$\%s$	0.822	0.770	0.437	0.824
h	0.954	0.797	0.595	0.571
b	0.805	0.861	0.636	0.859
d	0.765	0.763	0.411	0.822
$\%s^2$	0.957	0.993	0.966	0.988
h^2	0.941	0.878	0.987	0.458
b^2	0.900	0.784	0.754	0.925
d^2	0.983	0.973	0.903	0.986
$\%s \times h$	0.977	0.763	0.483	0.827
$\%s \times b$	0.924	0.798	0.511	0.823
$\%s \times d$	0.918	0.807	0.502	0.836
$h \times b$	0.993	0.816	0.876	0.886
$h \times d$	0.910	0.835	0.932	0.981
$b \times d$	0.844	0.994	0.997	0.957

Knowing that the displacements in the service condition are based on the useful span of the beams [19], in an attempt to improve the models previously obtained, the δs was also considered as an independent variable, which resulted in new adjustments for Fs, Fu, and δu, expressed by Equations (17)–(19), respectively, and the results of ANOVA in Table 8.

$$\begin{gathered} Fs = -15.06 + 246 \times \%s + 0.0607 \times h + 0.185 \times b + 2.20 \times d + 0.365 \times \delta s - \\ 570 \times \%s2 + 0.000154 \times h2 + 0.000853 \times b2 + 0.0065 \times d2 + 0.00576 \times \delta s2 - \\ 10.06 \times \%s \times h - 19.2 \times \%s \times b + 101 \times \%s \times d - 4.58 \times \%s \times \delta s + 0.00077 \times h \times b + \\ 0.00330 \times h \times d - 0.002264 \times h \times \delta s - 0.00016 \times b \times d - \\ 0.01156 \times b \times \delta s + 0.00697 \times d \times \delta s \\ \left[R^2 adj = 97.57\%\right] \end{gathered} \tag{17}$$

$$\begin{gathered} Fu = -42.8 - 318 \times \%s + 0.300 \times h + 0.440 \times b + 7.62 \times d + 1.077 \times \delta s + \\ 2703 \times \%s2 - 0.000016 \times h2 + 0.00098 \times b2 - 0.0235 \times d2 - 0.00857 \times \delta s2 - \\ 23.5 \times \%s \times h - 49.3 \times \%s \times b + 277 \times \%s \times d - 10.99 \times \%s \times \delta s - 0.00052 \times h \times b \\ + 0.00136 \times h \times d - 0.00289 \times h \times \delta s - 0.0001 \times b \times d - \\ 0.01020 \times b \times \delta s + 0.0301 \times d \times \delta s \\ \left[R^2 adj = 94.26\%\right] \end{gathered} \tag{18}$$

$$\begin{gathered} \delta u = -110.1 + 149 \times \%s + 1.155 \times h - 0.16 \times b + 13.9 \times d + 13.08 \times \delta s - \\ 5893 \times \%s2 - 0.00454 \times h2 - 0.0018 \times b2 - 0.020 \times d2 - 0.0784 \times \delta s2 - \\ 45 \times \%s \times h - 102 \times \%s \times b + 521 \times \%s \times d - 1.1 \times \%s \times \delta s + 0.0029 \times h \times b - \\ 0.0024 \times h \times d + 0.00401 \times h \times \delta s + 0.0071 \times b \times d - 0.0217 \times b \times \delta s + \\ 0.0017 \times d \times \delta s \\ \left[R^2 adj = 73.00\%\right] \end{gathered} \tag{19}$$

Table 8. ANOVA results (*p*-value) of the regression models expressed by Equations (12)–(14).

Statistics	Equation (6)	Equation (7)	Equation (8)
Model	0.000	0.000	0.000
Constant	0.004	0.000	0.174
$\%s$	0.351	0.171	0.718
h	0.866	0.432	0.643
b	0.696	0.272	0.600
d	0.294	0.130	0.716
$\delta\ s$	0.000	0.000	0.000
$\%s^2$	0.974	0.929	0.979
h^2	0.590	0.973	0.211
b^2	0.339	0.517	0.874
d^2	0.906	0.800	0.977
$\delta\ s^2$	0.060	0.098	0.044
$\%s \times h$	0.292	0.147	0.712
$\%s \times b$	0.371	0.174	0.705
$\%s \times d$	0.392	0.165	0.727
$\%s \times \delta s$	0.315	0.155	0.985
$h \times b$	0.415	0.746	0.809
$h \times d$	0.467	0.859	0.967
$h \times \delta s$	0.001	0.010	0.629
$b \times d$	0.979	0.993	0.928
$b \times \delta s$	0.000	0.000	0.113
$d \times \delta s$	0.286	0.007	0.984

Based on the terms considered significant by ANOVA presented in Table 8 and the hierarchy of the isolated terms, new regression models (hierarchical models) were generated, expressed in Equations (20)–(22).

The large reduction in terms from 21 to 6 in the Equation (17) model compared to the Equation (20) model had little impact on the adjusted determination coefficient, which decreased from 97.57% to 90.24%, showing the robustness of ANOVA as an analysis tool for the sensitivity of the terms of the models, and the same occurred with the models of Equations (13) and (14), which were changed

to Equations (13) and (14), respectively. Regarding the final displacement, the only independent variable considered significant by ANOVA was the limit displacement of the service condition.

$$Fs = -58.20 + 0.2142 \times h + 0.6890 \times b + 0.627 \times \delta s - 0.00205 \times h \times \delta s - 0.01111 \times b \times \delta s \quad \left[R^2 adj = 90.24\%\%\right] \tag{20}$$

$$Fu = -38.26 + 0.2467 \times h + 0.5429 \times b + 0.767 \times d + 0.329 \times \delta s - 0.00245 \times h \times \delta s - 0.00928 \times b \times \delta s + 0.01596 \times d \times \delta s \quad \left[R^2 adj = 93.61\%\right] \tag{21}$$

$$\delta u = -75.3 + 11.55 \times \delta s - 0.0784 \times \delta s^2 \quad \left[R^2 adj = 52.54\%\right] \tag{22}$$

Some authors have developed analytical and theoretical models to assess the increase in stiffness and the total load of beams reinforced with different materials. This research presented equations to estimate the service and ultimate loads and displacement of beams reinforced with steel bars positioned in the tensile and compression regions. The expressions presented coefficients of determination adjusted above 90% to estimate the last loads and above 70% to determine the ultimate displacement. With simplified expressions (Equations (20)–(22)), it was possible to estimate with good precision the service load and the ultimate load using parameters of the cross-section and the service limit displacement, showing the high applicability of the formulations. The results indicate that the expressions can be used to estimate load values of reinforced beams with parameters within the intervals analyzed in this work.

The results presented contribute to deepening the knowledge about beams reinforced with steel bars, analyzing the influence of different parameters on the load and displacement, and proposing expressions to estimate the loading of reinforced beams. However, more experimental and numerical studies with different reinforcement rates, different strengths of timber and reinforcement bars, and different beam dimensions are needed, aiming at more information to collaborate in the design of the structural project.

4. Conclusions

This study analyzed the mechanical behavior of GLT beams reinforced with symmetric steel bars. Based on the analysis of the results of the numerical models of beams subjected to bending, it can be concluded that:

- There was an average increase in the service load of 32% and 49% and in the ultimate load of 42.9% and 66.9% for reinforcement rates of 2% and 4%, respectively. The increased performance of reinforced members makes it possible to use elements with smaller heights, making it an alternative for projects with architectural restrictions;
- Beams with rates of 2% and 4% of reinforcement showed lower average displacements of 4.5% and 16.6%, respectively. With higher loads and lower maximum displacements, the reinforced beams showed a more ductile behavior;
- The models with 2% and 4% reinforcement rates showed statistically equivalent mean service force and ultimate force values. However, beams with a higher reinforcement rate showed higher values of forces and lower values of ultimate displacement; and
- Models for the estimation of service force, ultimate force, and ultimate displacement presented high adjusted coefficients of determination, with values of up to 97%. Such results indicate that the proposed models can be used to estimate such values, considering the lack of methodology and design guidelines for timber beams reinforced with steel bars.

The results confirmed the experimental evidence presented by other authors, which showed the efficiency of using steel bars in increasing beams' load capacity and ductile behavior. In addition, load and displacement estimation models have been proposed, contributing to the development of a methodology for dimensioning elements reinforced with steel bars. However, further studies with different types of wood, types of steel, dimensions, and loads are necessary.

Author Contributions: Conceptualization, A.F.F.G., L.T. and J.L.A.; methodology, F.J.R.M., H.F.d.S. and J.L.A.; software, A.L.C., A.F.F.G. and F.N.A.; validation, F.J.R.M. and H.F.d.S.; formal analysis, F.N.A. and J.L.A.; investigation, H.F.d.S. and L.T.; resources, F.J.R.M. and J.L.A.; data curation, F.N.A. and J.L.A.; writing—original draft preparation, A.F.F.G., F.N.A. and F.J.R.M.; writing—review and editing, A.L.C., F.N.A. and J.L.A.; visualization, A.F.F.G. and L.T.; supervision, A.L.C., H.F.d.S. and

J.L.A.; project administration, A.L.C. and H.F.d.S. All authors have read and agreed to the published version of the manuscript.

Funding: This research was funded by: CAPES (Coordenação de Aperfeiçoamento de Pessoal de Nível Superior–Finance Code 001), CNPq (Conselho Nacional de Desenvolvimento Científico e Tecnológico), and by the Pró-Reitoria de Pesquisa, Inovação e Pós-Graduação of Instituto Federal de Rondônia (PROPESP/IFRO).

Data Availability Statement: The data presented in this study are available on request from the corresponding authors.

Acknowledgments: We would like to acknowledge the Pró-Reitoria de Pesquisa, Inovação e Pós-Graduação of Instituto Federal de Rondônia (PROPESP/IFRO), and the Coordenação de Aperfeiçoamento de Pessoal de Nível Superior-Brazil (CAPES).

Conflicts of Interest: The authors declare no conflict of interest.

References

1. Wei, Y.; Zhou, M.Q.; Chen, D.J. Flexural behaviour of glulam bamboo beams reinforced with near-surface mounted steel bars. *Mater. Res. Innov.* **2015**, *19*, S1-98–S1-103. [CrossRef]
2. Fiorelli, J.; Rempe, N.; Molina, J.C.; Dias, A.A. Natural Fiber-Reinforced Polymer for Structural Application. In *Agricultural Biomass Based Potential Materials*; Springer: Cham, Switzerland, 2015; pp. 435–449. [CrossRef]
3. Allam, S.M.; Shoukry, M.S.; Rashad, G.E.; Hassan, A.S. Evaluation of tension stiffening effect on the crack width calculation of flexural RC members. *Alex. Eng. J.* **2013**, *52*, 163–173. [CrossRef]
4. Soriano, J.; Pellis, B.P.; Mascia, N.T. Mechanical performance of glued-laminated timber beams symmetrically reinforced with steel bars. *Compos. Struct.* **2016**, *150*, 200–207. [CrossRef]
5. De Lorenzis, L.; Scialpi, V.; La Tegola, A. Analytical and experimental study on bonded-in CFRP bars in glulam timber. *Compos. Part B Eng.* **2005**, *36*, 279–289. [CrossRef]
6. Yang, H.; Liu, W.; Lu, W.; Zhu, S.; Geng, Q. Flexural behavior of FRP and steel reinforced glulam beams: Experimental and theoretical evaluation. *Constr. Build. Mater.* **2016**, *106*, 550–563. [CrossRef]
7. Zhang, J.; Shen, H.; Qiu, R.; Xu, Q.; Gao, S. Short-Term Flexural Behavior of Prestressed Glulam Beams Reinforced with Curved Tendons. *J. Struct. Eng.* **2020**, *146*, 04020086. [CrossRef]
8. Vecchí, C.; Colajanni, S.; Deletis, R.; Catanese, A.; Iudicello, S. Reinforced glulam: An innovative building technology. *Int. J. Hous. Sci. Its Appl.* **2008**, *32*, 207–221.
9. Borri, A.; Corradi, M.; Grazini, A. A method for flexural reinforcement of old wood beams with CFRP materials. *Compos. Part B Eng.* **2005**, *36*, 143–153. [CrossRef]
10. Neubauerová, P. Timber Beams Strengthened by Carbon–Fiber Reinforced Lamellas. *Procedia Eng.* **2012**, *40*, 292–297. [CrossRef]
11. Ghanbari-Ghazijahani, T.; Russo, T.; Valipour, H.R. Lightweight timber I-beams reinforced by composite materials. *Compos. Struct.* **2019**, *233*, 111579. [CrossRef]
12. Raftery, G.M.; Whelan, C. Low-grade glued laminated timber beams reinforced using improved arrangements of bonded-in GFRP rods. *Constr. Build. Mater.* **2014**, *52*, 209–220. [CrossRef]
13. Raftery, G.M.; Kelly, F. Basalt FRP rods for reinforcement and repair of timber. *Compos. Part B Eng.* **2015**, *70*, 9–19. [CrossRef]
14. Luca, V.; Marano, C. Prestressed glulam timbers reinforced with steel bars. *Constr. Build. Mater.* **2012**, *30*, 206–217. [CrossRef]
15. McConnell, E.; McPolin, D.; Taylor, S. Post-tensioning of glulam timber with steel tendons. *Constr. Build. Mater.* **2014**, *73*, 426–433. [CrossRef]
16. Donadon, B.F.; Mascia, N.T.; Vilela, R.; Trautwein, L.M. Experimental investigation of glued-laminated timber beams with Vectran-FRP reinforcement. *Eng. Struct.* **2019**, *202*, 109818. [CrossRef]
17. Crespo, J.; Majano-Majano, A.; Lara-Bocanegra, A.J.; Guaita, M. Mechanical Properties of Small Clear Specimens of Eucalyptus globulus Labill. *Materials* **2020**, *13*, 906. [CrossRef]
18. Abaqus. *De Simulia Abaqus/CAE User's Guide*; Dassault Systèmes Simulia Corp.: Providence, RI, USA, 2016.
19. ABNT—Associação Brasileira de Normas Técnicas. *NBR 7190: Projeto de Estruturas de Madeira*; ABNT: Rio de Janeiro, Brazil, 1997; p. 107.
20. Chaudhari, S.V.; Chakrabarti, M.A. Modeling of concrete for nonlinear analysis Using Finite Element Code ABAQUS. *Int. J. Comput. Appl.* **2012**, *44*, 14–18.
21. Ferreira, M.R. Nonlinear Analysis by Finite Elements of Torsion-Reinforced Concrete Beams. Master's Dissertation, University of Beira Interior, Covilhã, Portugal, 2016.
22. Sandhass, A.; Stanzl-Tschegg, S.E. Numerical modelling of timber and timber joints: Computational aspects. *Wood Sci. Technol.* **2020**, *54*, 31–61. [CrossRef]
23. Liu, D.; Liu, H.; Chen, Z.; Liao, X. Structural behavior of extreme thick-walled cold-formed square steel columns. *J. Constr. Steel Res.* **2016**, *128*, 371–379. [CrossRef]

24. Dias, A.; Van de Kuilen, J.; Lopes, S.; Cruz, H. A non-linear 3D FEM model to simulate timber–concrete joints. *Adv. Eng. Softw.* **2007**, *38*, 522–530. [CrossRef]
25. Moses, D.; Prion, H. Stress and failure analysis of wood composites: A new model. *Compos. Part B Eng.* **2004**, *35*, 251–261. [CrossRef]
26. Chen, Z.; Ni, C.N.; Kuan, S.; Dagenais, C.; Kuan, S. WoodST: A Temperature-Dependent Plastic-Damage Constitutive Model Used for Numerical Simulation of Wood-Based Materials and Connections. *J. Struct. Eng.* **2020**, *146*, 14. [CrossRef]
27. Reiterer, A.; Stanzl-Tschegg, S.E. Compressive behaviour of softwood under uniaxial loading at diferent orientations to the grain. *Mech. Mater.* **2001**, *33*, 705–715. [CrossRef]
28. Tran, T.-T.; Thi, V.-D.; Khelifa, M.; Oudjene, M.; Rogaume, Y. A constitutive numerical modelling of hybrid-based timber beams with partial composite action. *Constr. Build. Mater.* **2018**, *178*, 462–472. [CrossRef]
29. Hill, R. A Theory of the Yielding and Plastic Flow of Anisotropic Metals. *Proc. R. Soc. Lond. Ser. A Math. Phys. Sci.* **1948**, *193*, 281–297.
30. Guan, Z.; Kitamori, A.; Komatsu, K. Experimental study and finite element modelling of Japanese "Nuki" joints—Part two: Racking resistance subjected to different wedge configurations. *Eng. Struct.* **2008**, *30*, 2041–2049. [CrossRef]
31. Guan, Z.; Zhu, E. Finite element modelling of anisotropic elasto-plastic timber composite beams with openings. *Eng. Struct.* **2009**, *31*, 394–403. [CrossRef]
32. Mackenzie-Helnwein, P.; Eberhardsteiner, J.; Mang, H.A. A multi-surface plasticity model for clear wood and its application to the finite element analysis of structural details. *Comput. Mech.* **2003**, *31*, 204–218. [CrossRef]
33. Xu, B.-H.; Bouchair, A.; Taazount, M.; Vega, E. Numerical and experimental analyses of multiple-dowel steel-to-timber joints in tension perpendicular to grain. *Eng. Struct.* **2009**, *31*, 2357–2367. [CrossRef]
34. Nowak, T.P.; Jasienko, J.; Nowak, T.; Czepizak, D. Numerical analysis of CFRP-reinforced wooden beams under bending. In Proceedings of the World Conference on Timber Engineering, Tentino, Italy, 20–24 June 2010.
35. Wang, M.; Song, X.; Gu, X. Three-Dimensional Combined Elastic-Plastic and Damage Model for Nonlinear Analysis of Wood. *J. Struct. Eng.* **2018**, *144*, 04018103. [CrossRef]
36. Oudjene, M.; Khelifa, M. Finite element modelling of wooden structures at large deformations and brittle failure prediction. *Mater. Des.* **2009**, *30*, 4081–4087. [CrossRef]
37. CEN—Comité Européen de Normalisation. *EN 338: Structural Timber—Strength Classes*; CEN: Brussels, Belgium, 2009.
38. Molina, J.C. Dynamic Behavior Analysis of the Bond Formed by Glued Steel Bars for Mixed Wooden and Concrete Trays for Bridges. Ph.D. Thesis, University of São Paulo, São Carlos, Brazil, 2008.
39. Dias, A.M.M.P.G. Mechanical Behavior of Timber-Concrete Joints. Ph.D. Thesis, University of Coimbra, Coimbra, Portugal, 2005.
40. Borri, A.; Corradi, M. Strengthening of timber beams with high strength steel cords. *Compos. Part B Eng.* **2011**, *42*, 1480–1491. [CrossRef]
41. Johnsson, H.; Blanksvard, T.; Carolin, A. Glulam members strengthened by carbon fiber reinforcement. *Mater. Struct.* **2007**, *40*, 47–56. [CrossRef]
42. Raftery, G.M.; Harte, A.M. Low-grade glued laminated timber reinforced with FRP plate. *Compos. Part B Eng.* **2011**, *42*, 724–735. [CrossRef]